Optical properties of Pd_2Si

M. Amiotti, G. Guizzetti, F. Marabelli, and A. Piaggi
Dipartimento di Fisica "A. Volta," Università degli Studi di Pavia, Via Bassi 6, I-27100 Pavia, Italy

V. N. Antonov,* Vl. N. Antonov,* O. Jepsen, and O. K. Andersen
Max-Planck-Institut für Festkörperforschung, D-7000 Stuttgart 80, Federal Republic of Germany

A. Borghesi and F. Nava
Dipartimento di Fisica, Università degli Studi di Modena, Via Campi 213/A, I-41100 Modena, Italy

V. V. Nemoshkalenko
Institute of Metal Physics, Kiev, U.S.S.R.

R. Madar and A. Rouault
Ecole Nationale Supérieure de Physique de Grenoble, Laboratoire des Matériaux et du Génie Physique, Boîte Postale 46, 38402 St. Martin d'Herès, France
(Received 21 November 1991)

Near-normal reflectivity measurements with polarized light have been performed on good quality single crystals of Pd_2Si in the spectral range from 0.05 to 4 eV. Moreover, spectral ellipsometry from 1.4 to 5 eV and nonpolarized reflectivity from 3 to 12 eV have been used in order to Kramers-Kronig analyze the data and to obtain the dielectric functions. The results show strong anisotropy in the optical response for the polarization along the crystallographic c axis, or in the basal plane, of the hexagonal cell, according to the transport measurements. The optical properties of Pd_2Si have been calculated within the local-density approximation using the semirelativistic linear-muffin-tin-orbital method. The band structure, the ℓ-projected densities of states, the complex dielectric function, the optical conductivity, the optical reflectivity, and the electron-energy-loss spectrum have been obtained in the energy range from 0 to 5 eV. The agreement with the experimental data is rather good.

I. INTRODUCTION

Palladium silicides were among the first silicide compounds to be used in optoelectronic devices and in silicon technology,[1,2] for example, as buffering layers for preventing the interdiffusion of silicon and other metals. Since then they have been intensively investigated both experimentally and theoretically by a number of techniques. In particular, ultraviolet and x-ray photoemission spectroscopies,[3–5] as well as Auger-electron spectroscopy,[6,7] extended x-ray-absorption fine structure[7,8] or electron-energy-loss spectroscopy[9] have been used to investigate the Pd local structure in the silicide formation and the electronic structure of the most stable phase which is the hexagonal Pd_2Si. Optical investigations have also been performed[10,11] both by reflectivity measurements and by ellipsometric techniques in order to obtain the refractive index and to characterize the electronic band structure of the material. These measurements have been obtained over a limited spectral range or with polycrystalline thin films. Differences between the properties of polycrystalline films and of single crystalline samples have been pointed out in a study of the transport properties[12] and they are essentially due to the larger disorder in polycrystalline samples. It would therefore be of interest to study the optical response along different directions of the hexagonal crystalline structure of Pd_2Si.

In this paper we give a detailed and consistent characterization of the electronic properties of Pd_2Si obtained, on the one hand, from accurate measurements on high-quality single crystals of the optical response, over a large spectral range (0.05–12 eV) with polarized light or ellipsometric techniques. On the other hand, they have been obtained from the theoretical calculation of the band structure and the dielectric functions which we can compare directly with experiments.

The electronic properties of Pd_2Si have been analyzed in Ref. 13. Using the linear-muffin-tin-orbital method (LMTO) in the atomic-sphere approximation (ASA), the energy bands, densities of states (DOS), x-ray-absorption spectra, and the total energy were determined.

II. CRYSTAL STRUCTURE

Pd_2Si crystallizes in a hexagonal structure (space group $P\hat{6}2m$) with nine atoms per unit cell (Fig. 1). Due to the fact that the two basal planes which are displaced by $c/2$ in the c direction display different atomic sites, there are two nonequivalent Si and Pd atoms in the unit cell. We shall label them by the index (1) or (2), respectively (Fig. 1). The measured lattice constants are

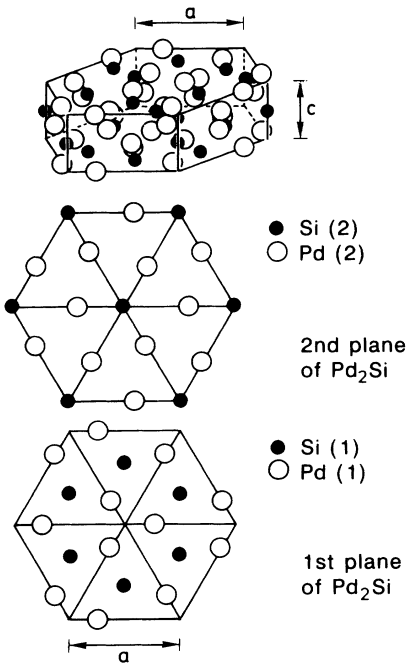

FIG. 1. Silicon and palladium atomic sites in the two alternating planes normal to the c axis and in the hexagonal cell in Pd_2Si. Both Si and Pd atoms are situated on two nonequivalent sites, labeled (1) and (2).

a=6.496 Å and c=3.435 Å,[12,14] with c/a= 0.5285. The Brillouin zone (BZ) is shown in Fig. 2, where the points and lines of high symmetry are labeled in accordance with the standard notation of Ref. 15.

III. EXPERIMENT

High-quality single crystalline samples of stoichiometric Pd_2Si have been prepared in Grenoble at the Laboratoire des Matériaux of the Ecole Nationale Supérieure de Physique. The details of the preparation and the structural characterization of the samples have been given elsewhere.[12]

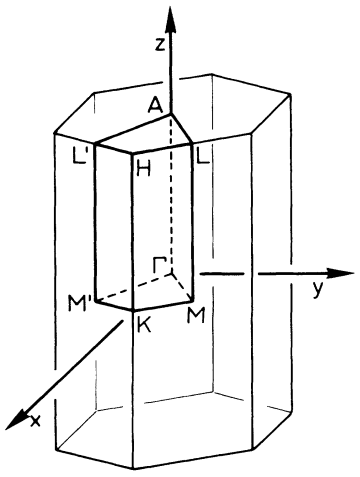

FIG. 2. The Brillouin zone for hexagonal Pd_2Si and its irreducible part.

We have two samples about 5×4×1.5 mm^3 large. One surface of each sample has been prepared for optical measurements by usual mechanical polishing with corundum and diamond powder. The polished surface of the first sample lies in the basal plane, whereas for the second it is in a plane including the crystallographic c axis. We verified that the measurements obtained on the first surface were equivalent to the measurements performed with light polarized perpendicularly to the c axis in the second sample.

Optical reflectivity at near normal incidence has been measured at photon energy from 50 meV up to 0.6 eV by a Fourier spectrometer Bruker IFS 113v, using a gold mirror as a reference. From 0.5 up to 4 eV the absolute reflectivity has been measured with a self-made grating spectrometer equipped with a Zeiss double monochromator. All the measurements have been performed with light polarized along the direction parallel and, respectively, perpendicular to the c axis of the hcp structure of Pd_2Si. We used a grid polarizer with a KRS5 substrate for the infrared and a polarizing beam splitter for the visible range of energy.

In the photon energy range from 1.4 to 5 eV we obtained both the real (n) and the imaginary (k) part of the refraction index directly from an ellipsometric measurement performed with a SOPRA instrument model MOSS ES4G.

Converting the ellipsometric data in terms of reflectivity values, we found very good agreement with the measured reflectivity in the range of energies where the spectra overlap.

We also performed reflectivity measurements from 4 to 12 eV with a McPherson spectrometer using nonpolarized light. Whereas the contribution of the light polarized in the basal plane ($e \perp c$) has been easily obtained by measuring the sample with the optical surface lying in this plane, the spectrum concerning the polarization along the c axis ($e \parallel c$) has been calculated from the measurements on both samples. Indeed, the intensity of the light reflected by the surface containing the c axis is given by $I_R = \frac{I_\parallel + I_\perp}{2}$ (actually, we measured I_R as an average on different positions of the sample, in order to avoid spurious effects due to polarization of the light in the spectrometer). The results obtained above 5 eV are not completely satisfactory; we have to shift these spectra towards higher reflectivity values in order to link the curves with the low-energy and the ellipsometric measurements. This can be ascribed to a loss of intensity due to the high diffusion of light in vacuum ultraviolet. Then the high-energy data have to be taken into consideration with some care. Anyway, the addition to the spectra of this high-energy part improves the Kramers-Kronig analysis of the data considerably, permitting to reobtain, in the range 1.4–5.0 eV, the ellipsometric values with very good precision (discrepancies are smaller than 1%) without paying great attention to the extrapolation of the data at higher energies (a common extrapolation

in ω^{-4} has been used).

Kramers-Kronig transformations have been applied to the reflectivity in order to obtain the refraction indexes and the dielectric functions over the whole measured spectral range.

No extrapolation has been used at low energies due to sufficient low-energy limit and to the regular shape of the experimental data. The use of an extrapolation towards the reflectivity of 1 at zero frequency, based on the Hagens-Rubens relation $R = 1 - \sqrt{\frac{2\omega}{\pi\sigma_{dc}}}$, which connects the value of the dc conductivity to the low-energy reflectivity, does not affect the results beyond $\omega = 0.1$ eV.

IV. THEORY

The calculated optical spectra of Pd_2Si in the energy range from 0 to 5 eV were obtained from the electronic energy bands and wave functions using the local approximation to the density-functional theory (LDA).[16] Although the LDA aims to describe the ground-state properties only, we shall also use it for the electronic excitations, first of all because this is presently the only *ab initio* approach for *d*-band metals and their compounds, and because past experience indicates that it gives results which are typically accurate to within about 0.5 eV for metals with broad bands.

A detailed description of the LMTO-ASA method which we have used, including its application to the electronic structure of compounds, is given elsewhere.[17,18] The present calculations were carried out in a semirelativistic approach and with basis functions including angular momenta up to l=3 for palladium and l=2 for silicon. The "frozen-core" approximation was adopted and the core charge distributions were evaluated from the solutions of the Dirac equation for free atoms. The **k**-integrated functions have been evaluated by the tetrahedron method[19] on a grid of 216 **k** points in the irreducible part of the Brillouin zone (BZ).

The linear response of a system to an external electromagnetic field with small wave vector is determined by the imaginary part $\epsilon_2(\omega)$ of the complex dielectric function $\tilde{\epsilon}(\omega) = \epsilon_1(\omega) + i\epsilon_2(\omega)$. We have calculated the dielectric function for frequencies well above those of the phonons and therefore we considered only electronic excitations. For these we used the random-phase approximation and neglected local-field and finite lifetime effects.[20] The dielectric function is a tensor, but by an appropriate choice of the principal axes we could diagonalize it and restrict our considerations to the diagonal matrix elements $\tilde{\epsilon}^{\nu\nu}(\omega)$, with $\nu = x, y, z$. The interband contribution to the imaginary part of the dielectric function $\epsilon_2(\omega)$ is given by

$$\epsilon_2^{\nu\nu}(\omega) = \frac{8\pi^2 e^2}{m^2\omega^2} \sum_{n}^{\text{unocc}} \sum_{n'}^{\text{occ}} \int_{\text{BZ}} |P_{nn'}^{\nu}(\mathbf{k})|^2 \times \delta(E_n^{\mathbf{k}} - E_{n'}^{\mathbf{k}} - \hbar\omega) \frac{d^3k}{(2\pi)^3}, \quad (1)$$

where ν is the direction of the electric field, $E_n^{\mathbf{k}}$ are the one-electron energies, and $P_{nn'}^{\nu}(\mathbf{k})$ are the momentum matrix elements.

After having evaluated $\epsilon_2(\omega)$ we calculated the interband contribution to the real part of the dielectric function $\epsilon_1(\omega)$ from the Kramers-Kronig relation:

$$\epsilon_1(\omega) = 1 + \frac{2}{\pi} P \int_0^{\infty} \frac{\epsilon_2(\omega')\omega' d\omega'}{\omega'^2 - \omega^2}, \quad (2)$$

where P stands for principal value. Finally, we obtained the total complex dielectric function by adding the intraband contribution. We have neglected this contribution to $\epsilon_2(\omega)$ according to the perfect crystal approximation (the defects and lattice oscillations are absent). The intraband contribution to $\epsilon_1(\omega)$ is given by

$$\epsilon_1^{\nu\nu}(\omega)|_{\text{intra}} = 1 - \frac{(\omega_p^{\nu\nu})^2}{\omega^2}, \quad (3)$$

where the squared plasma frequency is given by

$$(\omega_p^{\nu\nu})^2 = \left(\frac{e}{\pi\hbar}\right)^2 \sum_n \int_{\text{BZ}} \left(\frac{\partial E_n^{\mathbf{k}}}{\partial k^{\nu}}\right)^2 \delta(E_n^{\mathbf{k}} - E_F) d^3k. \quad (4)$$

In this work we have calculated the complex dielectric function, the optical conductivity $\sigma(\omega)$, the reflectance $R(\omega)$, and the electron-energy-loss spectrum $L(\omega)$ using the relations (1)–(4) and the following expressions:

$$\sigma(\omega) = \frac{\omega}{4\pi}\epsilon_2(\omega), \quad (5)$$

$$R(\omega) = \left|\frac{\sqrt{\tilde{\epsilon}(\omega)} - 1}{\sqrt{\tilde{\epsilon}(\omega)} + 1}\right|^2, \quad (6)$$

$$L(\omega) = \text{Im}\left\{\frac{-1}{\tilde{\epsilon}(\omega)}\right\} = \frac{\epsilon_2(\omega)}{\epsilon_1^2(\omega) + \epsilon_2^2(\omega)}. \quad (7)$$

V. RESULTS AND DISCUSSION

A. Experimental results

The measured reflectivity spectra, as well as the dielectric functions obtained from the Kramers-Kronig transformation, are shown in Fig. 3 and Figs. 4 and 5, respectively.

For both polarizations the reflectivity spectra show metallic behavior at the lowest energies, with high reflectivity values approaching unity for frequencies decreasing towards zero. For $e \perp c$ the reflectivity decreases monotonically for increasing energies up to about 2 eV; then it shows a maximum at about 2.5 eV and, for higher energies, continues to decrease. Regarding the polarization $e \parallel c$, the spectrum shows high reflectivity for energies below 1 eV, followed by a rapid decrease to a minimum at 1.2 eV. Two structures appear at 1.7 and 2.7 eV, respectively, and after these the reflectivity decreases for increasing energies. For both polarizations the reflectivities reach a broad minimum at about 9 eV.

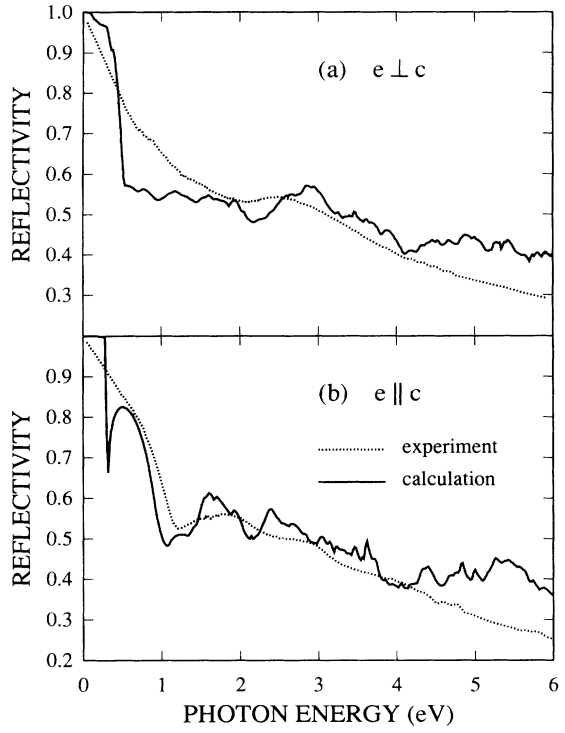

FIG. 3. The measured and calculated optical reflectivity in Pd_2Si.

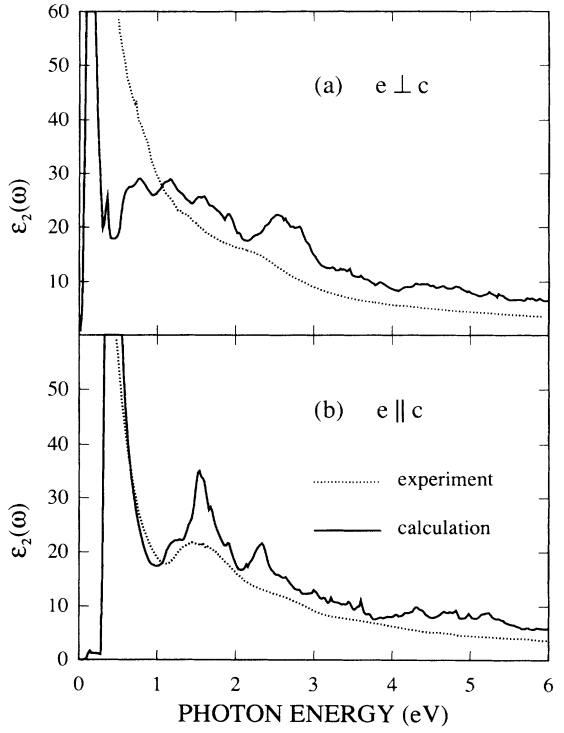

FIG. 5. The imaginary part ϵ_2 of the dielectric function in Pd_2Si.

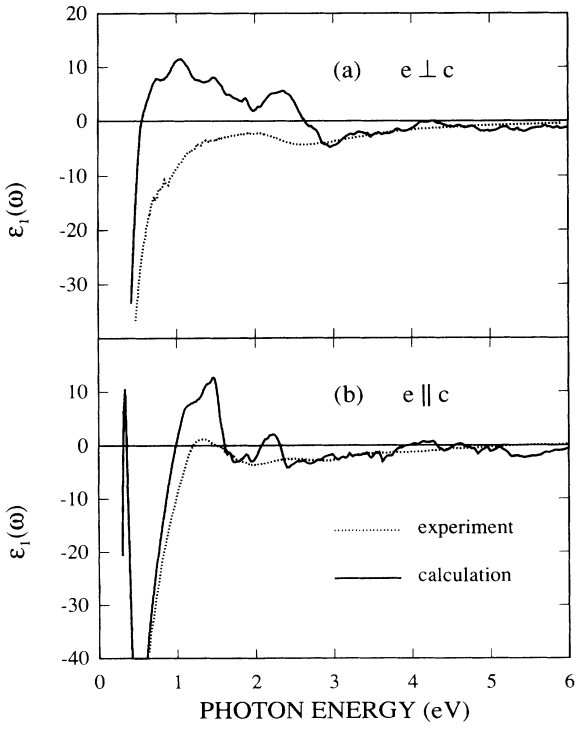

FIG. 4. The real part ϵ_1 of the dielectric function in Pd_2Si.

We note that the optical spectra previously obtained on Pd_2Si polycrystalline films[10,11] qualitatively agree with our measurements for $e \perp c$; in particular the smooth structure at about 2.3 eV is observed in all these measurements. Such a feature can be ascribed to a preferred growth orientation of the microcrystals in the thin films. The intensities are slightly different, being higher than our results in Ref. 10 and, respectively, lower in Ref. 11.

The behavior of the reflectivity is reflected in the real (ϵ_1) and imaginary (ϵ_2) parts of the dielectric function. For the polarization $e \parallel c$, ϵ_2 shows two structures over the free-carrier contribution, respectively, at 1.4 and 2.5 eV. For $e \perp c$ only one broad structure appears at 2.2 eV. From the analysis of the free-carrier part at very low energy (below 0.2 eV) in terms of a Drude model, one can infer the values of the plasma frequency and of the damping parameter γ (or the scattering time $\tau = 1/\gamma$). The complex dielectric constant is

$$\tilde{\epsilon} = \epsilon_1 + i\epsilon_2 = \left(\epsilon_\infty - \frac{\omega_p^2}{\omega^2+\gamma^2}\right) + i\left(\frac{\omega_p^2\gamma}{\omega(\omega^2+\gamma^2)}\right) . \tag{8}$$

In the region where $\epsilon_\infty \ll \frac{\omega_p^2}{\omega^2}$ the plasma frequency ω_p can be easily obtained from the slope of $1/\epsilon_1$ versus ω^2 and the damping γ from the ratio $\frac{\omega\epsilon_2}{\epsilon_1}$.

The determination of γ is subject to a large uncertainty due to its very strong dependence on the absolute value of

the reflectivity in the low-energy region. Furthermore, it shows a frequency dependence also at these low energies and we can infer from both polarizations only one value of $\gamma = 0.03 \pm 0.01$ eV.

The obtained plasma frequencies are $\omega_{p\parallel} = 3.6$ eV and $\omega_{p\perp} = 2.8$ eV, for the electric field parallel and perpendicular to the c axis. These compare well with our calculated values of $\omega_{p\parallel}$=3.69 eV and $\omega_{p\perp}$=3.36 eV, when the experimental uncertainty and the approximations in the calculations are taken into account.

The results are in very good agreement with the measured dc resistivity;[12] in particular the ratio $(\frac{\omega_{p\parallel}}{\omega_{p\perp}})^2$ ($\simeq 1.6$), is equal to the ratio of the resistivities. Then, as argued in the study of the resistivity, the anisotropy in the transport properties depends essentially only on the different effective number of carriers, or the different effective mass of the carriers, along the two crystallographic directions.

An estimate of these masses in the model of one parabolic band can be obtained by using the expression[12]

$$\rho_{\mathrm{sat}\parallel,\perp} = \frac{2v_F}{\omega^2_{p\parallel,\perp}\lambda} , \tag{9}$$

where the saturation resistivity at high temperatures ρ_{sat} is taken, in the appropriate units, from Ref. 12, the mean free path λ is assumed equal to the interatomic distance d=2.48 Å, and the Fermi velocity $v_F = \sqrt{v_\parallel^2 + 2v_\perp^2}$. Assuming a paraboloid as Fermi surface, with Fermi vectors $k_{Fz} = k_{F\parallel} \neq k_{Fx} = k_{Fy} = k_\perp$, it is easy to calculate the masses $m^*_\parallel = 1.1m_e$ and $m^*_\perp = 1.8m_e$ and the carrier concentration n=1.05×10^{22} cm^{-3}. Actually, the Fermi surface is much more complicated, being composed of several different toroidal and open surfaces, so a direct comparison of these values with the theory is not possible.

B. Theoretical results

1. Energy bands and density of states

The calculated band structure of Pd_2Si (Fig. 6) is in good agreement with previous calculations.[13] Three low-lying bands centered around −11 to −8 eV are of mainly Si s character and separated by an energy gap from the rest of the bands. The remaining part of the filled bands is characterized by a very high density of states. These flat bands have mainly Pd d character and their high density of states is connected with the large number of palladium atoms per unit cell. The total and partial DOS's are presented in Figs. 7 and 8, respectively. The total DOS contains the contribution from all nine atoms in the unit cell, i.e., from 3 Pd(1), 3 Pd(2), 2 Si(1), and 1 Si(2) atoms. The Fermi level (E_F) is located in the dip of the DOS curve, so that the density of states at E_F is rather small. The s electrons of silicon are located near the valence-band bottom whereas the p states of silicon in the occupied part of the valence band are strongly hybridized with the d states of palladium. Above E_F the d states of palladium have some admixture of silicon p states. The f states of palladium and d states of silicon are mainly situated far above E_F. It is interesting to

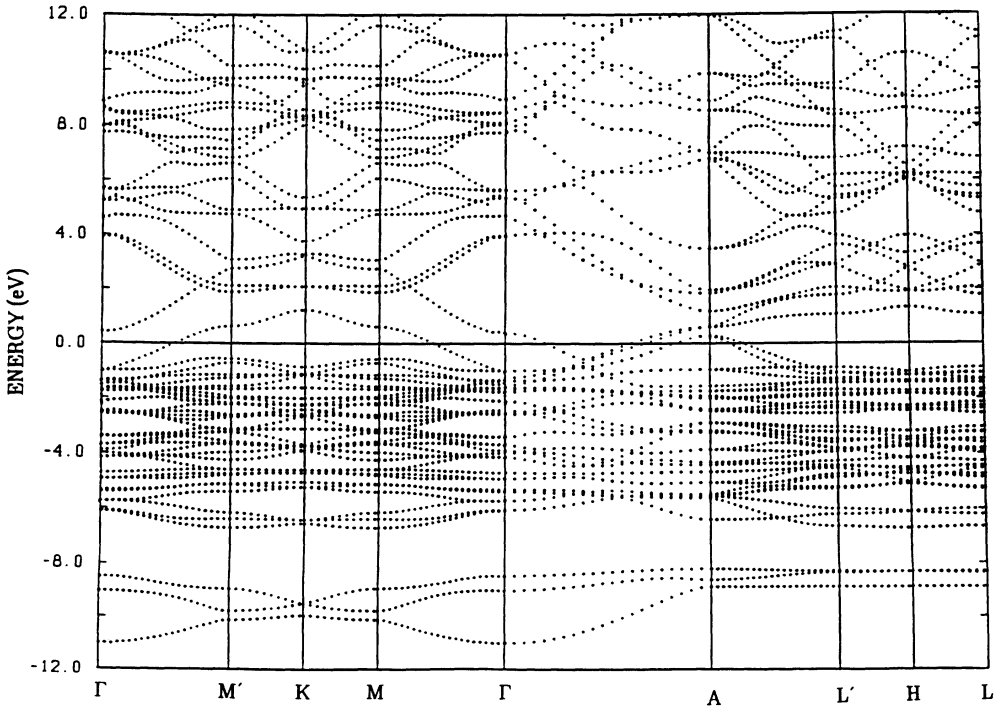

FIG. 6. Self-consistent energy-band structure of Pd_2Si along the high-symmetry lines shown in Fig. 2.

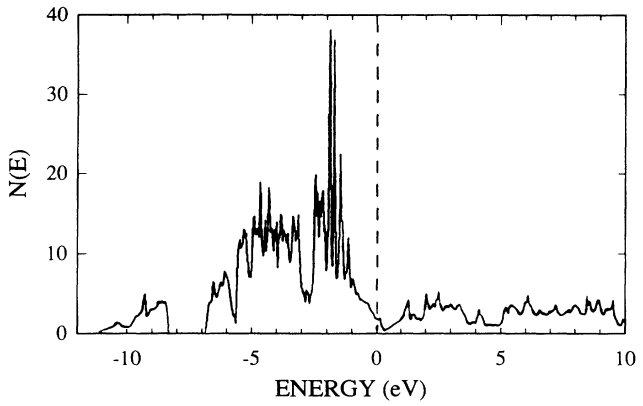

FIG. 7. Self-consistent total density of states $N(E)$ of Pd_2Si in units of number of states/(cell eV).

analyze the differences between Pd(1) and Pd(2) and between Si(1) and Si(2) partial DOS's. Figure 8 shows the similarity between the two inequivalent Pd atoms and the two inequivalent Si atoms. A few differences in the spectral shape may be noticed. For example, the d states below E_F are more peaked in Pd(2) than in Pd(1) due to the larger coordination number of Pd(1) compared with Pd(2). Figure 9 shows the details of the energy-band structure of Pd_2Si near the Fermi level. Only four energy bands (which we shall label with numbers from 35 to 38) cross the Fermi level. Along the Γ-M symmetry direction only energy-band number 37 crosses E_F. The 35th and 36th energy bands cross the Fermi level along the A-L direction. These two bands are degenerated and cross the Fermi level along the Γ-A line. Along this line the 37th and 38th energy bands also cross E_F. As will be shown below, the main contribution to the optical conductivity in the infrared and visible spectral regions comes from the interband transitions between these energy bands in the vicinity of the symmetry point A and the symmetry lines Γ-A and A-L.

2. *Optical properties and comparison with experiment*

In our theoretical investigation, we first calculate directly the imaginary part of the dielectric function [Eq. (1)]. This can be interpreted in terms of interband transitions. A very large anisotropy of the optical properties of Pd_2Si was found from both experiment and theory. Figure 10 shows the calculated $\epsilon_2(\omega)$ of Pd_2Si for two different light polarizations $e \parallel c$ and $e \perp c$. There are four maxima in $\epsilon_2(\omega)$ which all, except the first one which appears only in the $e \perp c$ polarization, originate from the same interband transitions for both polarizations. The difference in intensity for the two polarizations is due to the transition matrix element. Within the 0–3-eV range there are only four possible initial-state–final-state bands with band numbers from 35 to 38. The main character of the energy bands numbers 35 and 36 along the A-L line is Pd(1)(z, xz, yz), Pd(2)$(x, y, xy, x^2-y^2, 3z^2-r^2)$, Si(1)$(s, x, y, x^2-y^2, xy)$, Si(2)$(z, yz, xz)$. The character along the Γ-A line is, for the doubly degenerate 35th-36th bands, mainly Pd(1)(x, z, xz, yz), Pd(2)(x, y, xz, xy), Si(1)(x, xz, xy), Si(2)(x, y, yz, xz, x^2-y^2), for the 37th band Pd(1)(x, y, xz, yz, x^2-y^2), Pd(2)$(x, y, xy,$

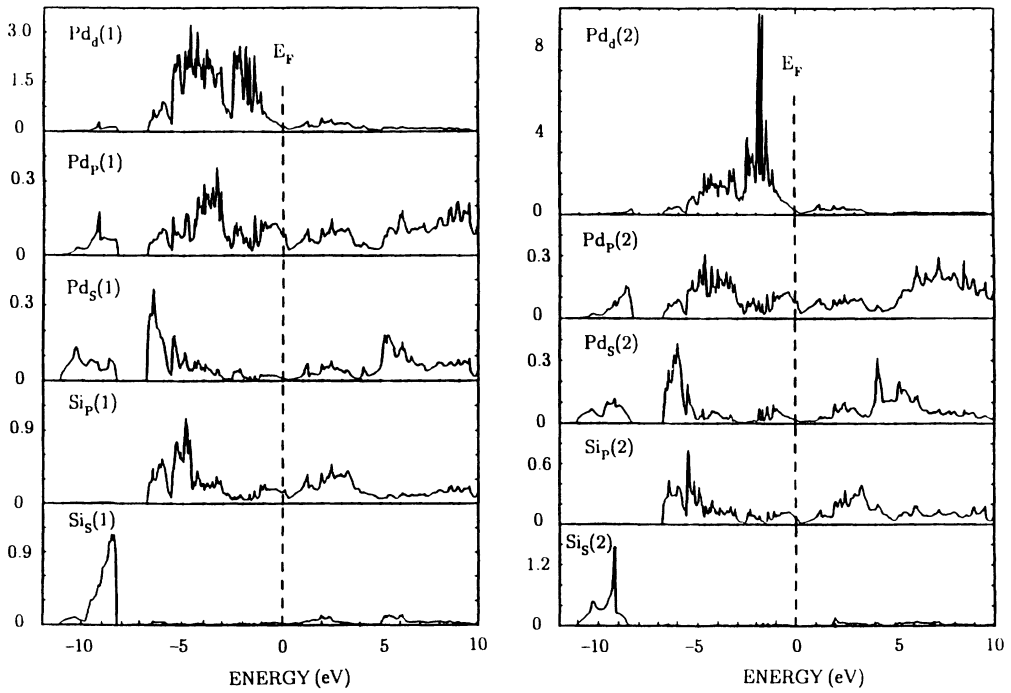

FIG. 8. Self-consistent partial densities of states of Pd_2Si in units of states/(atom eV).

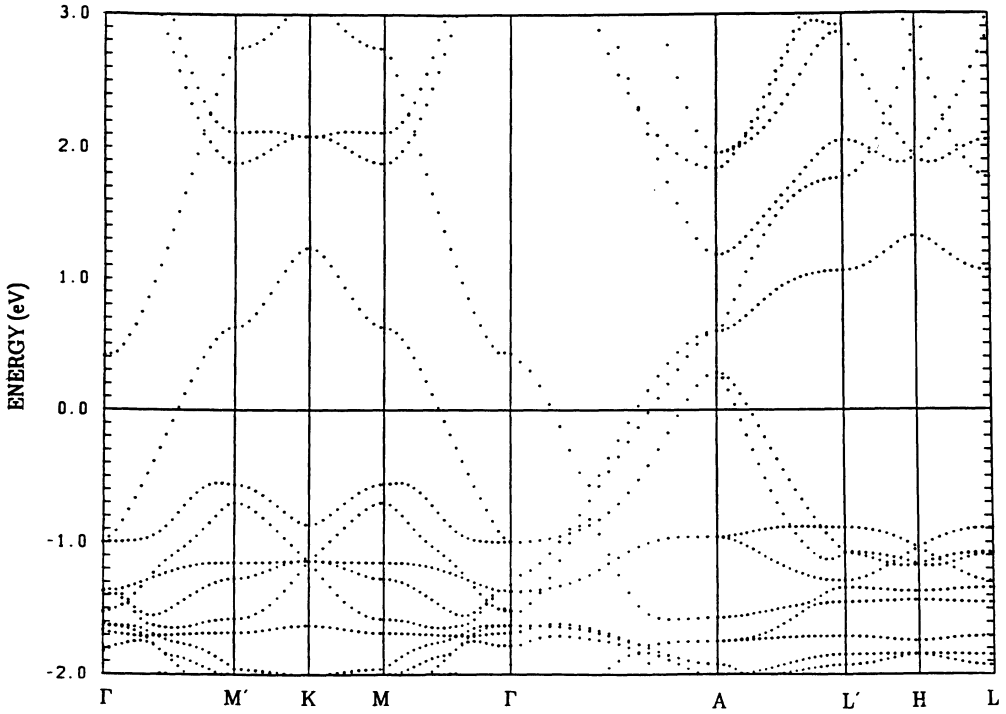

FIG. 9. Self-consistent energy band structure of Pd_2Si near the Fermi energy and along the high-symmetry lines shown in Fig. 2.

$xz, yz, x^2 - y^2$), Si(2)($z, 3z^2 - r^2$), and for the 38th band Pd(1)($x, y, x^2 - y^2, yz$), Pd(2)(xy, yz, xz), Si(1)(z), Si(2)(s). The strong maximum in the $e \perp c$ polarization at 0.15 eV is due to the 35 → 36 interband transitions along the A-L symmetry direction with contributions from the matrix elements: $< z|y|yz >$ and $< z|x|xz >$ on Pd(1); $< x|y|xy >$, $< y|x|xy >$, $< x|x|x^2 - y^2 >$, $< x|x|3z^2 - r^2 >$, $< y|y|x^2 - y^2 >$, and $< y|y|3z^2 - r^2 >$ on Pd(2); $< x|x|s >$, $< y|y|s >$, $< x|x|x^2 - y^2 >$, $< x|y|xy >$, $< y|x|xy >$, and $< y|y|x^2 - y^2 >$ on Si(1), and $< z|y|yz >$, $< z|x|xz >$, $< yz|y|z >$, and $< xz|x|z >$ on Si(2). The most intensive second maximum in the $e \parallel c$ at 0.4 eV is formed by transitions from the 35th-36th to the 37th energy band in the Γ-A symmetry direction with contributions from the matrix elements: $< x|z|xz >$, $< x|x|x^2 - y^2 >$, $< z|x|xz >$, $< z|y|yz >$, $< xz|z|x >$, and $< yz|z|y >$ on Pd(1); $< x|z|xz >$, $< x|y|xy >$, $< x|x|x^2 - y^2 >$, $< y|x|xy >$, $< y|y|x^2 - y^2 >$,$< y|z|yz >$, $< xy|y|x >$, $< xy|x|y >$, and $< xz|z|x >$ on Pd(2); $< x|x|3z^2 - r^2 >$, $< y|y|3z^2 - r^2 >$, $< yz|y|z >$, and $< xz|x|z >$ on Si(2). These transitions give contributions for both polarizations. Due to the size of the optical transition matrix elements the intensity of the transitions $< i|z|f >$ is several times larger than that of the $< i|x, y|f >$ transitions. The $\epsilon_2(\omega)$ for $e \parallel c$ polarization has a threshold at 0.08 eV in contrast to the $e \perp c$ polarization (Fig. 10). The infrared interband transitions near zero energy (in $e \perp c$) are due to the existence of the doubly degenerate 35th-36th energy band crossing the Fermi level along the Γ-A symmetry direction. Moving away from the Γ-A symmetry line the doubly degenerate 35th-36th energy bands split and they have the following characters: The 35th band has mostly Pd(1)($xy, x^2 - y^2$), Pd(2)($x, y, xz, xy, yz, x^2 - y^2$), and Si(2)($s, z$) character, and the 36th band has mostly Pd(1)($x, y, x^2 - y^2, yz, xz, xy$), Pd(2)($x^2 - y^2, xy$), Si(1)($s$), and Si(2)($s$) character. The 35 → 36 interband transitions are manifested only in the $e \perp c$ polarization [matrix elements: $< xy|y|x >$, $< x^2 - y^2|x|x >$, $< xy|x|y >$, $< x^2 - y^2|y|y >$, on Pd(1),

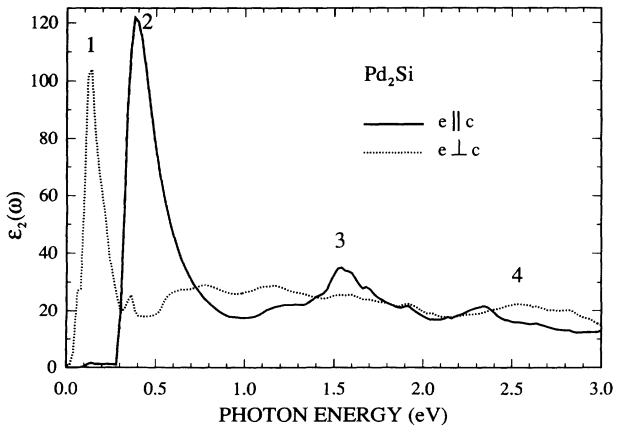

FIG. 10. The calculated imaginary part ϵ_2 of the dielectric function in Pd_2Si for low energies.

and $< x|x|x^2 - y^2 >$, $< x|y|xy >$, $< y|y|x^2 - y^2 >$, $< y|x|xy >$ on Pd(2)]. The peak number 3 at 1.5 eV comes from the 33 → 36; 35 → 37,38, and 36 → 38 interband transitions. The fourth broad feature around ~ 2.5 eV is formed by transition from the 36th to the 39th energy band and 31,32 → 37 transitions in both polarization.

In Figs. 3–5 we compare the calculated optical properties [optical reflectivity $R(\omega)$, $\epsilon_1(\omega)$, and $\epsilon_2(\omega)$] with experiment for both polarizations. As may be seen there is good overall agreement between theory and experiment. The strong interband transition at 0.4 eV in the $e \parallel c$ polarization leads to the very narrow peak in $\epsilon_{1\parallel}(\omega)$ and the local minimum in $R_\parallel(\omega)$ at 0.35 eV. These fine structures are smoothed by the finite-lifetime effects, lattice imperfections, and distortions. Therefore, only a smooth, but still distinguishable, shoulder is observed in the experimental curves. The low-energy peak at 0.15 meV in the $e \perp c$ polarization is not seen in $\epsilon_{1\perp}(\omega)$ and $R_\perp(\omega)$ because this transition occurs at too small energy and is suppressed by the intraband transitions [Drude term in $\epsilon_{1\perp}(\omega)$]. Consequently, the strong anisotropy of $\epsilon_1(\omega)$ and $R(\omega)$ in the 0–1-eV energy range can be explained by the anisotropy of the interband transitions. The theory also predicts a strong anisotropy of $\epsilon_{1\parallel}(\omega)$ and $\epsilon_{1\perp}(\omega)$ above 0.4 eV which goes through zero at 1.0 and 0.58 eV, respectively. The second sign change of $\epsilon_{1\parallel}(\omega)$ and $\epsilon_{1\perp}(\omega)$ occurs at 1.62 and 2.64 eV. In this case the change in the sign of $\epsilon_{1\parallel}(\omega)$ and $\epsilon_{1\perp}(\omega)$ reflects only the anomalous dispersion of these functions in the region of interband absorption. Although the experimental $\epsilon_{1\perp}(\omega)$ remains negative in this region, the shapes of the experimental curves reflects reasonably well the features of the theoretical ones. The calculated $\epsilon_{1\parallel}(\omega)$ and $\epsilon_{1\perp}(\omega)$ vanish again at an energy larger than 20 eV. Since in this range the imaginary part of the dielectric function is very low, the conditions for the plasma resonance are satisfied. There are strong resonance maxima at this energy in the calculated electron-energy-loss spectra $L(\omega)$ for both polarizations.

VI. CONCLUSIONS

The characterization of the optical properties of Pd_2Si has been carried out over a wide spectral range. A strong anisotropy has been found both in the experiments and in the calculations between the optical response for light polarization perpendicular and parallel to the crystallographic c axis of the hexagonal cell. Experimental results for $e \perp c$ are in qualitative agreement with old measurements performed on polycrystalline films.

The anisotropy is particularly strong in the infrared spectra, from which the plasma frequencies $\omega_{p\parallel}$=3.6 and $\omega_{p\perp}$=2.8 eV have been obtained for the intraband excitations. The theoretical analysis of the calculated bands and matrix elements in the vicinity of the Fermi level shows that the huge low-lying peaks in $\epsilon_{2\parallel}(\omega)$ and $\epsilon_{2\perp}(\omega)$ at, respectively, 0.4 and 0.15 eV originate from different optical transitions. A close correspondence between theory and experiment is found for the structures at 1.5 and 2.5 eV ($e \parallel c$) and at 2.3 eV ($e \perp c$). The band-structure calculations also show that the bands involved in these transitions are formed essentially from hybridized palladium d states and silicon p states.

ACKNOWLEDGMENTS

This work was partially supported by Progetto Finalizzato "Materiali e Dispositivi per l'Elettronica a Stato Solido" and by Gruppo Nazionale Struttura della Materia del Consiglio Nazionale delle Ricerche, Italy. Two of us (V.N.A. and Vl.N.A.) would like to thank the MPI FKF for hospitality during their stay in Stuttgart.

*Permanent address: Institute of Metal Physics, Ukrainian Academy of Sciences, Vernadskogo 36, 252142 Kiev, U.S.S.R.

[1] J. T. Lue, Solid State Electron. **26**, 787 (1983).
[2] H. Elabd and W. F. Kosonocky, RCA Rev. **43**, 568 (1982).
[3] J. F. Freeouf, J. W. Rubloff, P. S. Ho, and T. S. Kuan, Phys. Rev. Lett. **43**, 1886 (1979).
[4] A. Franciosi and J. H. Weaver, Phys. Rev. B **27**, 3554 (1983).
[5] G. Rossi, I. Lindau, L. Braicovich, and I. Abbati, Phys. Rev. B **38**, 3031 (1983).
[6] P. S. Ho, G. W. Rubloff, J. E. Lewis, V. L. Moruzzi, and A. R. Williams, Phys. Rev. B **22**, 4784 (1980).
[7] M. De Crescenzi, E. Colavita, U. Del Pennino, P. Sassaroli, S. Valeri, C. Rinaldi, L. Sorba, and S. Nannarone, Phys. Rev. B **32**, 612 (1985).
[8] J. Stöhr and R. Jaeger, J. Vac. Sci. Technol. **21**, 619 (1982).
[9] S. Nannarone, A. M. Fiorello, U. del Pennino, C. Mariani, M. G. Betti, and M. De Crescenzi, J. Vac. Sci. Technol. A **5**, 1474 (1987).
[10] Juh Tzang Lue, Hong-Wen Chen, and Shwa-Ing Law, Phys. Rev. B **34**, 5438 (1986).
[11] A. Borghesi, G. Guizzetti, L. Nosenzo, A. Piaggi, A. Stella, and G. Majni, Semicond. Sci. Technol. **1**, 184 (1986).
[12] R. Marani, F. Nava, A. Rouault, R. Madar, and J. P. Senateur, J. Phys. Condens. Matter **1**, 5887 (1989).
[13] O. Bisi, O. Jepsen, and O.K. Andersen, Phys. Rev. B **36**, 9439 (1987).
[14] N. N. Matyushenko, Poroshk. Metall. **1**, 20 (1964).
[15] C. J. Bradley and A. P. Cracknell, *The Mathematical Theory of Symmetry in Solids* (Clarendon, Oxford, 1972).
[16] U. Barth and L. Hedin, J. Phys. C **4**, 2064 (1971).
[17] O. K. Andersen, Phys. Rev. B **12**, 3060 (1975).
[18] H. L. Skriver, *The LMTO Method* (Springer, Berlin, 1984).
[19] O. Jepsen and O. K. Andersen, Solid State Commun. **9**, 1763 (1971).
[20] H. Ehrenreich and M. H. Cohen, Phys. Rev. **115**, 786 (1959).